Chemistry–A European Journal
Research Article
doi.org/10.1002/chem.202301550
Chemistry Europe
European Chemical Societies Publishing
www.chemeurj.org

Through-Space, Lone-Pair Promoted Aromatic Substitution: A Relay Mechanism Can Beat Out Direct Activation

Muhammad Kazim,[a, d] Zhitao Feng,[b] Srini Vemulapalli,[c] Maxime A. Siegler,[a] Anant Chopra,[a] Phuong Minh Nguyen,[a] Maxwell Gargiulo Holl,[a] Liangyu Guan,[a] Travis Dudding,*[c] Dean J. Tantillo,*[b] and Thomas Lectka*[a]

Abstract: We report a detailed experimental and theoretical analysis of through-space arene activation with halogens, tetrazoles and achiral esters and amides. Contrary to previously assumed direct activation through σ-complex stabilization, our results suggest that these reactions proceed by a *relay* mechanism wherein the lone pair-containing activators form exothermic π-complexes with electrophilic nitronium ion before transferring it to the probe ring through low barrier transition states. Noncovalent interactions (NCI) plots and Quantum Theory of Atoms in Molecules (QTAIM) analyses depict favorable interactions between the Lewis base (LB) and the nitronium ion in the precomplexes and the transition states, suggesting directing group participation throughout the mechanism. The regioselectivity of substitution also comports with a relay mechanism. In all, these data pave the way for an alternate platform of electrophilic aromatic substitution (EAS) reactions.

Introduction

Electrophilic aromatic substitution (EAS) constitutes one of the most important classes of transformations in the entirety of chemical synthesis.[1,2] To the present day, synthetic chemists rely heavily on traditional methods of attaching activating (or deactivating) groups directly to aromatic rings to control the rates and selectivities of substitutions. Imagine instead a functional group containing a lone pair of electrons suspended over the π-cloud of an aromatic ring. Theoretically, such an arrangement should activate the aromatic ring to approach of an electrophile (Scheme 1). In order to test this hypothesis, our laboratory has employed rigid bicyclic structures based on fused 9,10-dihydroanthracene-bicycloheptane scaffolds to lock select heteroatoms (e.g., fluorine, oxygen) in close spatial proximity to aromatic rings.[3,4] The results were dramatic; the probe ring was functionalized almost exclusively, and intermolecular experiments indicated several hundred-fold rate enhancements (Scheme 2).

Mechanistically, we assumed a *direct* activation of the probe ring by the proximate group that would in turn release electron density into the ring in the transition state (Scheme 3, I). We modeled and rationalized this process (somewhat crudely as it were) through the calculation of the corresponding "Wheland" intermediates, or σ-complexes,[5] as they often seemed to account for the observed selectivities. We also sought enlightenment in an examination of electrostatic potential surfaces and HOMO coefficients. As can be seen in Figure 1, the

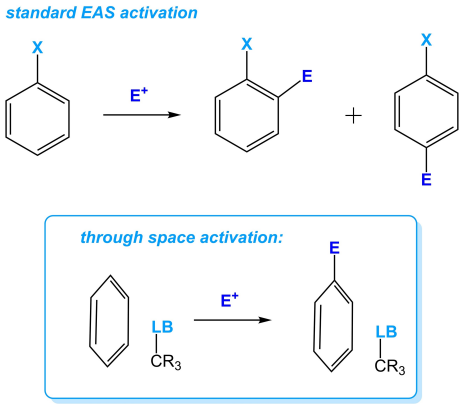

Scheme 1. Paradigms of electrophilic aromatic substitution.

[a] Dr. M. Kazim, Dr. M. A. Siegler, A. Chopra, P. Minh Nguyen, Dr. M. Gargiulo Holl, Dr. L. Guan, Prof. T. Lectka
Department of Chemistry
Johns Hopkins University
3400 N. Charles St., Baltimore, MD 21218 (USA)
E-mail: lectka@jhu.edu

[b] Z. Feng, Prof. D. J. Tantillo
Department of Chemistry
University of California
1 Shields Ave, Davis, CA 95616 (USA)
E-mail: djtantillo@ucdavis.edu

[c] S. Vemulapalli, Prof. T. Dudding
Department of Chemistry
Brock University
1812 Sir Isaac Brock Way, St. Catharines, ON L2S 3A1 (Canada)
E-mail: tdudding@brocku.ca

[d] Dr. M. Kazim
Current address: Chemical Biology Laboratory, National Cancer Institute, Frederick, MD 21702 (USA)

Supporting information for this article is available on the WWW under https://doi.org/10.1002/chem.202301550

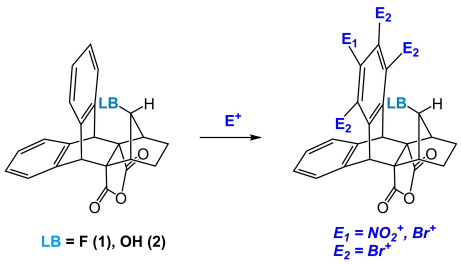

Scheme 2. Original model system.

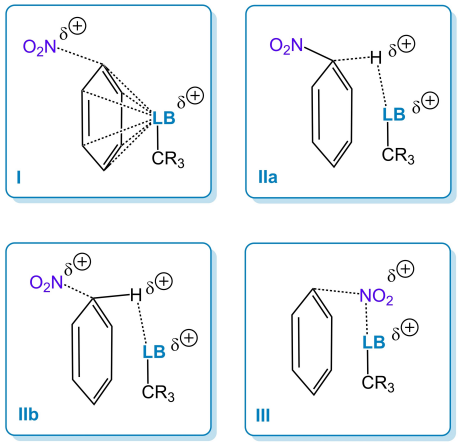

Scheme 3. Possible modes of mechanisms; direct activation through σ-complex stabilization (Types I, II) vs. relay mechanism (Type III).

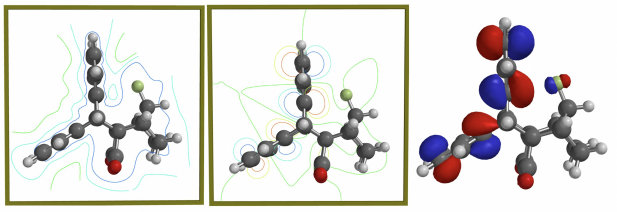

Figure 1. Slice of electrostatic potential surface coincident with the plane of symmetry of **1** (left); HOMO slice (center); and HOMO (right).

superficial differences between the probe aromatic rings and the control aromatic rings in **1** are subtle and can hardly be used to rationalize the dramatic outcomes.

Our initial approach to the problem turned out to be naive if not incorrect. For example, one can conceive of several other modes of activation, including rate-determining deprotonation (Scheme 3, IIa)[6,7] and stabilization of the transition state through hydrogen bonding (Scheme 3, IIb). In this paper, we show through experiment and calculation an even more surprising result – namely, *precomplexation*[8] of the electrophile to the LB, which thus serves as a relay to the aromatic ring (Scheme 3, III). We clarify and advance this work by the examination of other scaffolds and several more basic functional groups that would appear to favor precomplexation, as the structural rigidity of our original system precluded significant variation.

Background

We surmised that crystal structures would provide a wealth of information on the natural disposition of potential through-space directing groups with respect to aromatic rings. The Isostar program (CCDB) was employed to measure close contacts between aromatic rings and functional groups (Figure 2). Clearly, potential through-space activators show different oriental preferences with respect to the π face of aromatic rings, thus necessitating a detailed study of their impact on aromatic substitutions.

One important mechanistic hint for us was provided by Schneebeli and coworkers, who reported a remarkable diastereoselective nitration in a simple, abiotic system using chiral auxiliaries with carboxyethyl appendages.[9–12] They proposed that these groups, when appropriately located, can also act as internal bases by interacting with the aromatic proton being substituted in the σ-complex (Scheme 3, Type II) besides stabilizing its positive charge. More intriguingly, they observed a noncovalent interaction between the nitronium ion and the activator in the corresponding Wheland intermediate calculated

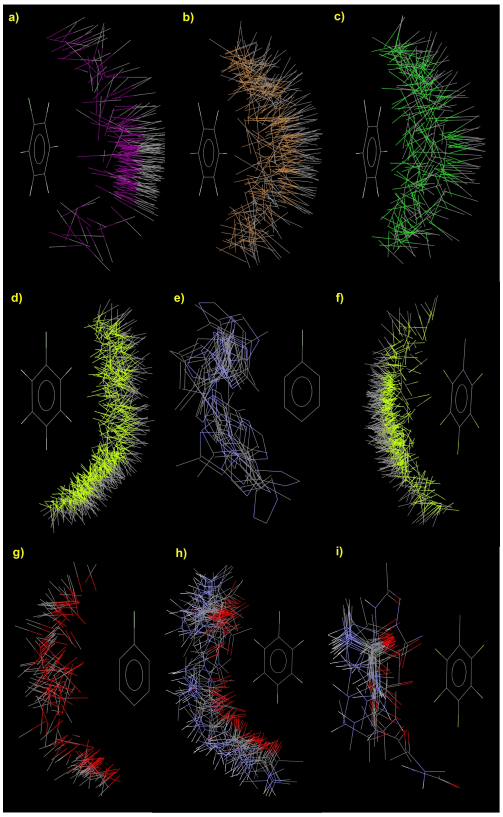

Figure 2. Close contacts (shorter than 0.16 Å of the sum of the van der Waals distances) of functional groups in crystals [CCDB] with aromatic rings. a) C–I/Ph group. b) C–Br/Ph. c) C–Cl/Ph. d) C–F/Ph. e) imidazole ring/Ph. f) C–F/C_6F_5 group. g) C–OH/Ph. h) amide/phenyl. i) amide/C_6F_5.

with density functional theory (DFT), if nitration were to occur *syn* to the activator (Figure 3).[9,10]

Our prior work and the results of Schneebeli's group prompted us to examine through-space arene activation with halogens, tetrazoles, esters and amides as activating groups. Our results led us to a model in which the reaction proceeds through a relay mechanism with activating groups containing lone pairs of electrons. The electrophile forms an exothermic π-complex with the activator before being transferred to the proximate aromatic ring; the resulting low-barrier transition state is stabilized by simultaneous interaction with the directing group (Figure 4a). This mechanism occurs in preference to the previously assumed direct activation through σ-complex stabilization. The positioning of the directing group is important; if it is too far away, its ability to serve as a stabilizing relay is foreclosed (Figure 4b). The strength of the relay interaction is also a consideration (Figure 4c). Halogens are expected to be "light touches," whereas amide and tetrazole groups should be strong binders.

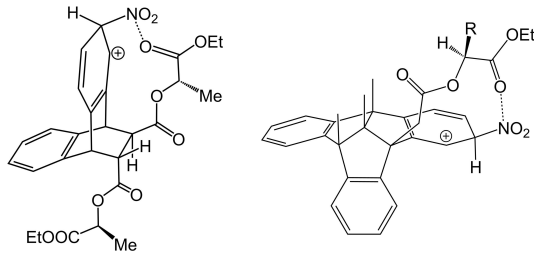

Figure 3. Noncovalent interactions between NO_2^+ and the ester carbonyl group in the Wheland intermediates obtained through syn-nitration calculated by Schneebeli and coworkers.[9,10]

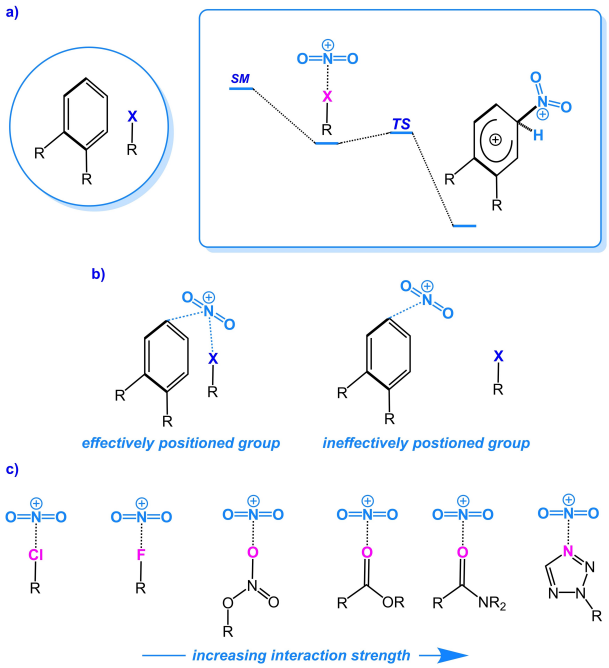

Figure 4. a) Energy diagram for precomplexation leading to a Wheland intermediate. The barrier height of the transition state (TS) may be either above or below the energy of the precomplex. b) Positioning of relay groups. c) Interactions of Lewis bases with nitronium ions.

Singleton and co-workers showed that modeling the regioselectivity of toluene nitration in water required careful consideration of the solvent complex coupled to molecular dynamics simulations, as a result of the flat potential (and free) energy surfaces associated with electrophilic addition.[13] Our computational results also point to fairly flat potential energy surfaces around the transition states through which activator $-NO_2^+$ π-complexes transform into σ-complexes that also make it challenging to predict the regioselectivity, although very illuminating when we do succeed in correlating theory and experiment (see below). Although a complete picture of regioselectivity may require exhaustive dynamic trajectory calculations of the very complex (relative to toluene or *o*-xylene) molecules involved here (beyond our current resources), our analysis helps rationalize these transformations and provides a practical model of predictive value.

Results and Discussion

Model systems

Our original model system (scaffold I) had the virtue of rigidly positioning the Lewis basic site very close to the probe ring. Unfortunately, we could only synthesize analogues containing fluoro and hydroxy groups. Related scaffold II afforded more choices, although the trade-off is that the Lewis base is positioned somewhat further from the probe ring. The third scaffold allows the placement of biologically relevant Lewis bases such as amides and esters (Figure 5).

Directed arene activation in scaffold I

Our original model (scaffold I) located heteroatoms in spatial proximity to the *top* aromatic ring while the *bottom* ring served as a control.[3,4] Interestingly, when compound **2** was subjected to nitrating conditions, the OH group formed a nitrate ester before substitution occurred on the probe ring, thereby providing us the first hint of a possible relay mechanism (Scheme 4).[3] Nevertheless, the nitrated alcohol still directs electrophilic nitration on the probe ring, in the presence of additional nitronium ions. In the case of compound **1**, however,

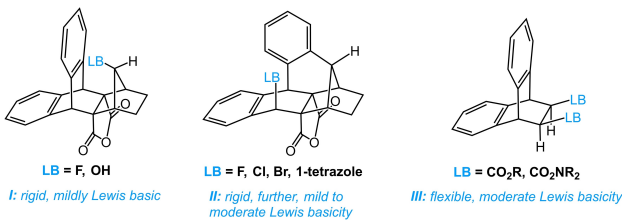

Figure 5. Representative model systems I, II, and III.

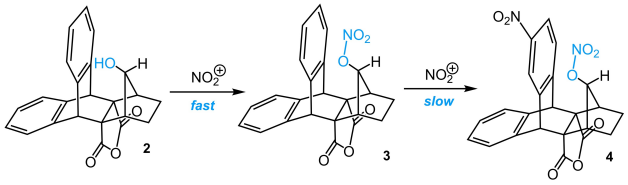

Scheme 4. Formation of nitrate ester **3** and its subsequent nitration.

experimental observations provided no outward sign of a relay mechanism.

Scaffold II

A serendipitous discovery[14–18] led to a new, somewhat more flexible scaffold. We attempted to generate $\mathbf{4a_1}$ (Figure 6), stabilized by a cation-π interaction, as a characterizable species.[19] Nevertheless, $\mathbf{4a_1}$ was but a fleeting reactive intermediate that rearranged under all circumstances to $\mathbf{4b_1}$, which then can trap a nucleophile. In hindsight, this was no surprise, as benzylic $\mathbf{4b_1}$ is predicted to be roughly 4 kcal/mol lower in energy than $\mathbf{4a_1}$.

Treatment of **5** with Xtalfluor-E exclusively resulted in the formation of "*up*" isomer 6 (Scheme 5) as confirmed by the ^{19}F NMR of isolated product (observed −160 ppm, DFT predicted −160 ppm and −215 ppm for *up* and *down* isomers). When subjected to nitrating conditions,[20] 6 predominantly nitrates the "*top*" ring at the positions indicated in Scheme 5 (~ 1.7 : 1 for **7a** : **7b**).

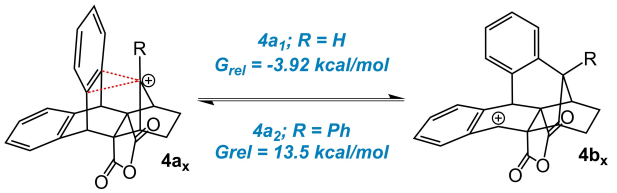

Figure 6. Relative Gibbs free energies of carbocations $\mathbf{4a_1}$//$\mathbf{4b_1}$ and $\mathbf{4b_1}$//$\mathbf{4b_2}$ at ωB97XD/6-311G(d,p).

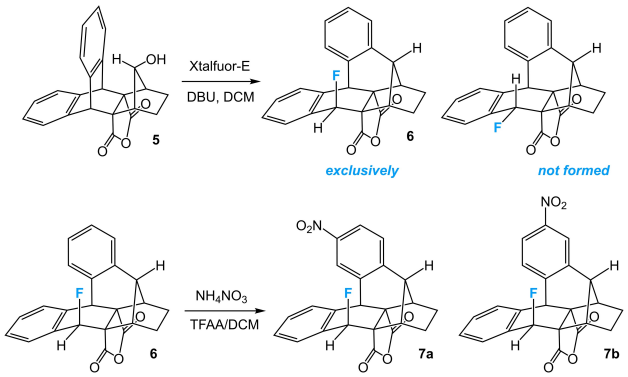

Scheme 5. Synthesis and nitration of compound **6** (**7a** : **7b** = ~1.7 : 1).

As a first approximation, we performed energetic analysis of σ-complexes which predicts those derived from the "*top*" ring to be roughly 8.6 kcal/mol lower in energy than those anchored on the *bottom* ring. At the same level, however, σ-complexes at the *top* ring were predicted to be roughly 5.2 kcal/mol lower in energy in **1**,[4a] despite the shorter distance of the fluorine atom from the positively charged carbon atom of the probe ring. Quite possibly, the *bottom* ring in **6** is being affected by the inductive effects of fluorine (see below).

Alternatively, we imagined replacing the hydrogen atom in **6** (H_A, Scheme 5) with a Ph group to provide an additional control ring free of steric as well as inductive effects. However, we feared that tertiary cation $\mathbf{4a_2}$ (Figure 6) might not be prone to rearrangement since both $\mathbf{4a_2}$ and $\mathbf{4b_2}$ are benzylic, and $\mathbf{4a_2}$ benefits from an additional cation–π interaction.[21–23] DFT optimization reveals $\mathbf{4b_2}$ to be roughly 13.5 kcal/mol *higher* in energy than $\mathbf{4a_2}$. However, nucleophilic attack on tertiary carbocation $\mathbf{4a_2}$ from inside is blocked by the stacked aromatic ring, whereas outside attack adds severe steric strain to the system. Experimentally, a rearrangement is observed, and **10** is produced exclusively upon treatment of alcohol **9** with Xtalfluor-E, which in turn was synthesized by a Grignard reaction of ketone **8** (Scheme 6).[3a] As observed previously, the ^{19}F NMR of the isolated product shows a peak at −162 ppm that is consistent with the calculated fluorine chemical shift for the *up* isomer. X-ray analysis confirms the structure in which the fluorine atom rests 2.83 Å from the nearest carbon atom on the adjacent aromatic ring (ring **A**, Scheme 6), a slightly greater distance than in compound **1** (2.68 Å).[4a] This molecule serves as another candidate for our investigation as it provides two control rings **B** and **C**, wherein **C** is free from ring strain and inductive effects, although its reactivity is relatively diminished by mono-, as opposed to disubstitution.

Subjecting **10** to nitrating conditions resulted in two major products **11a** and **11b** (~1.5 : 1) with nitrations predominately on the probe ring **A** (Scheme 7). The exact positions of the nitro groups were confirmed by X-ray crystallographic analysis (Scheme 7). ^{1}H NMR analysis of the reaction mixture, however, also revealed some unreacted **10** and very small amounts of dinitrated products whose characterization remained untrace-

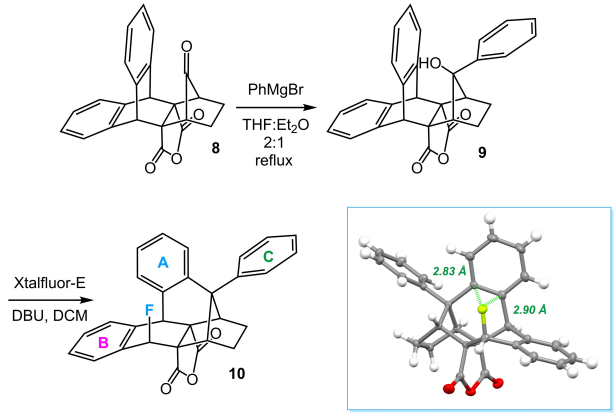

Scheme 6. Synthesis of compound **10**.

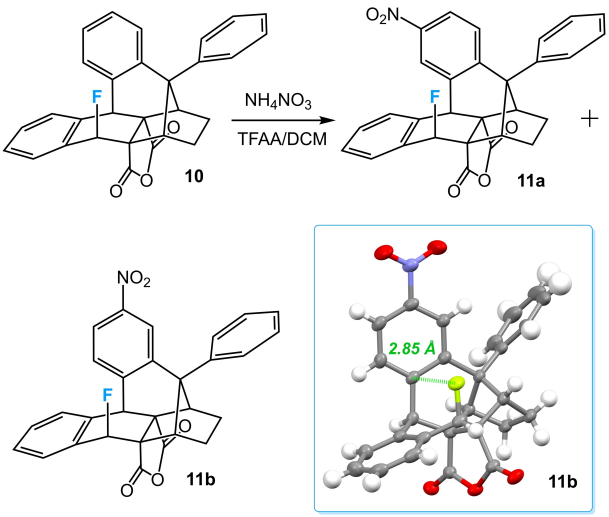

Scheme 7. Nitration of **10** and the X-ray crystal structure of **11 b** (50% probability level) (**11 a**:**11 b** = ~1.5:1).

able owing to trace impurities. We believe that they correspond to subsequent nitration of control ring **C**, after initial nitration of the probe ring.

Once again, DFT calculations predict the σ-complexes of the probe ring to be roughly 8 kcal/mol more favorable than those of both control rings. By this measure, we should not have observed formation of dinitrated products before **10** was completely nitrated, thereby providing another hint at the insufficiency of σ-complex analysis.

We then synthesized the rearranged chloride **12** by treating alcohol **9** with thionyl chloride (Scheme 8). Once again, the *up* orientation was confirmed by X-ray analysis, which locates the chlorine atom 3.08 Å (vs. 2.82 Å for fluorine) from the nearest carbon atom on the probe ring. Upon subjecting **12** to nitration, reaction occurs predominantly on the probe ring to form **14 a** and **14 b**, along with small amounts of inseparable dinitrated products (Scheme 8), thereby presenting the first putative indication of chlorine's ability to activate aromatic rings.

Attempted synthesis of the bromo-analogue by the treatment of alcohol **9** with thionyl bromide resulted in the formation of *top*-brominated compound **15**;[24] which upon nitration, exclusively substituted ring **C**, as confirmed by X-ray analysis of the isolated product (Scheme 9). By analogy, we imagine that the inseparable dinitrated byproducts observed in the nitrations of **10** and **12** contain the second nitro group on control ring **C**. This is in contrast to previously observed tetrabromination of alcohol **2**.[3a] The result, in retrospect, is not surprising as alcohols are generally stronger Lewis bases than bromides. In any case, bromide is not a good directing group.

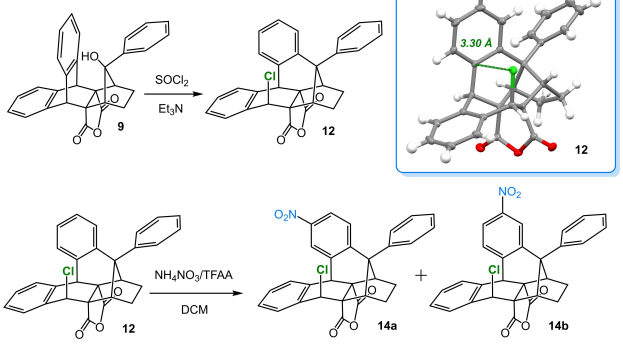

Scheme 8. Synthesis of **12**, its X-ray crystal structure (50% probability level) and its nitration.

Tetrazoles

The structural rearrangement of secondary carbocation **4 b** provided an attractive means to incorporate larger moieties within scaffold II. Tetrazoles, for instance, constitute an important class of organic molecules in medicinal chemistry, stemming from their isosterism with carboxylic acids and their metabolic stabilities.[25–32] While literature on their biological activities as well as physical properties is bountiful, their effect on aromatic reactivity is not as well-explored.

To this end, we synthesized rearranged tetrazole **18** by elaborating alcohol **5** (Scheme 10). DFT calculations predict two

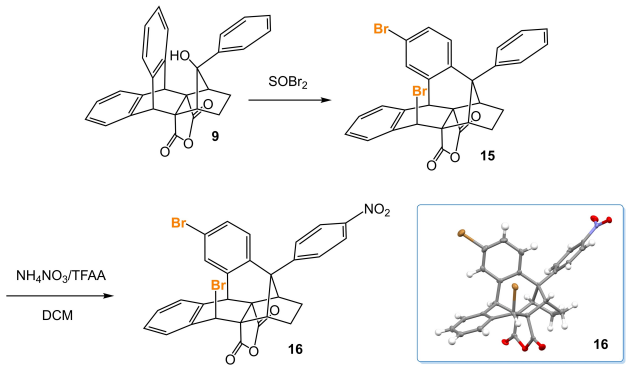

Scheme 9. Synthesis and nitration of the dibrominated analogue **15**.

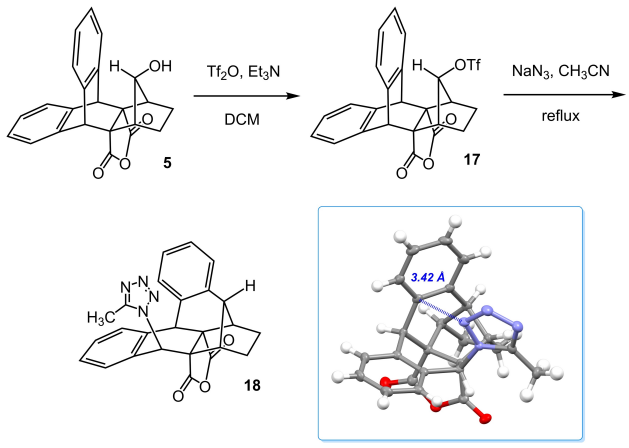

Scheme 10. Synthesis of tetrazole **18** and its crystal structure (50% probability level).

rotamers of **18** with an energy difference of 1.1 kcal/mol, connected by a rotational barrier of 9.8 kcal/mol. In rotamer **A**, N^2 of the tetrazole moiety is pointing towards the top ring as the 5-methyl group points out, whereas in rotamer **B**, the plane of the tetrazole moiety is almost parallel to the top ring as the 5-methyl group rests above the bottom ring.

In the ^{1}H NMR spectrum of the product, the methyl protons appear at 2.55 ppm (vs 2.49 ppm in 5-methyl-1H-tetrazole);[33] thus not in the anisotropic region of the bottom ring. It suggests that treating **17** with sodium azide in refluxing acetonitrile produced compound **18** as its **A** rotamer (Scheme 10). The structure was finally confirmed by X-ray analysis that located N^2 of the tetrazole moiety 3.17 Å away from the nearest carbon on the probe ring. When subjected to nitration, tetrazole **18** underwent exclusive reaction of the probe ring, predominantly on positions 2 and 3, as confirmed by X-ray analysis of the isolated products (Scheme 11).

Carbonyl directed arene activation: failure of the wheland model

Our investigation of carboxyalkyl group mediated arene activation began with attempted nitration of monoester 20.[34] Unfortunately, a mixture of inseparable nitrated products was observed in the ^{1}H NMR of the reaction mixture, most likely due to the asymmetry of the molecule.

When we synthesized *cis*-diester 21[35] as a symmetrical variant, we observed the exclusive nitration of the probe ring at

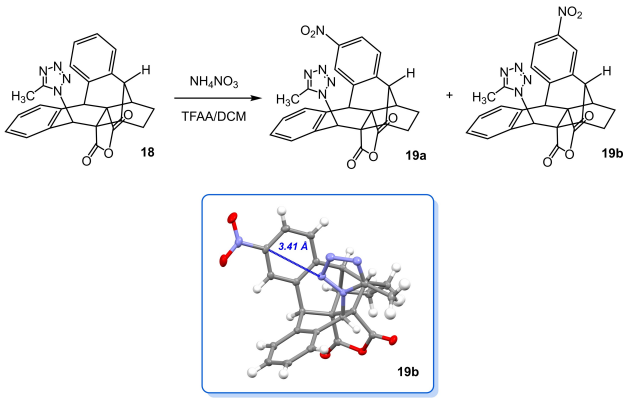

Scheme 11. Nitration of tetrazole **18** and the X-ray structure of **19b** (50% probability level).

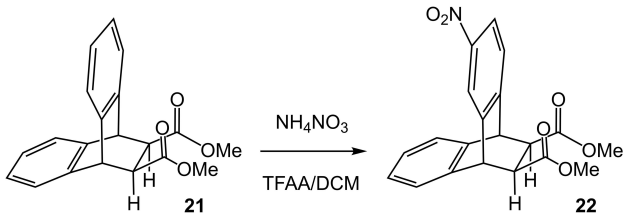

Scheme 12. Nitration of cis-diester **21**.

the "meta-para" position (Scheme 12). The structure of the product was confirmed by a [^{1}H,^{1}H]-NOESY spectrum[36,37] of the isolated material. No through-space coupling is observed between the aromatic protons of the substituted ring and the carbonyl α-protons (Figure 7).

Next, we turned to more Lewis basic amides. This is an inherently interesting case as it possesses biochemical relevance, given the multitude of close spatial interactions of amides with aromatic groups in proteins. We also reckoned that amides should exhibit stronger through-space arene activation. Optimized structures of the σ-complexes of amide 23 predict that the carbonyl group bends down to stabilize the positive charge on the proximate probe ring (O···C distance = 1.52 Å). As a result, 24bσ is predicted to be ~22 kcal/mol lower in energy than σ-complexes on the unperturbed ring. σ-Complex analysis also predicts a very strong regiochemical bias for nitration on the probe ring at the position *para* to the methylamido group (also about 20 kcal/mol). Thus, this substrate provides a test as to the viability of the crude Wheland analysis.

We synthesized **23** by functionalization of monoester **20**, which in turn yielded exclusive nitration of the probe ring at the positions indicated in Scheme 13 (~1:1 ratio for **24a**:**24b**) as confirmed by the [^{1}H,^{1}H]-NOESY spectrum of the isolated products, wherein no aromatic proton on the substituted ring engages in through-space coupling with the amide α-proton. *This result represents a clear failure of the Wheland analysis.* By this juncture, we had already developed some skepticism that simple σ-complex analysis could provide a good energetic picture of this reaction, and concluded that a more realistic approach would be called for (see below).

We also synthesized amide **25** (Scheme 13), which contains two additional, freely-rotating control aromatic rings in order to address the structural constraints associated with **23**. Once again, we observed exclusive nitration of the probe ring as confirmed by X-ray crystallographic analysis of isolated products (Scheme 13, ~1:1 ratio for **26a**:**26b**).

Finally, to confirm *actual* amide participation in these reactions, we synthesized control imide **27**,[38,39] whose structural restraints lock both carbonyl oxygens farther from and

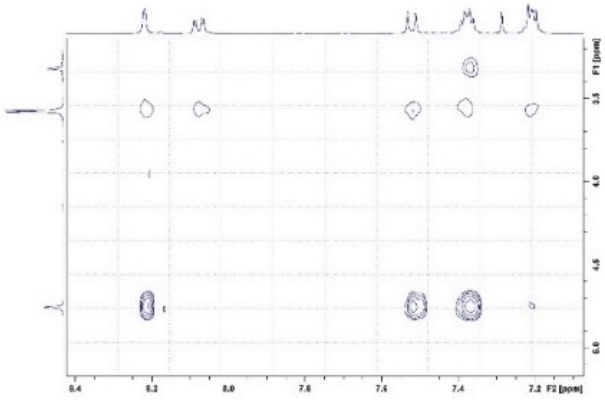

Figure 7. [^{1}H,^{1}H]-NOESY spectrum of 22 revealing no through-space coupling between the substituted ring to carbonyl-alpha protons.

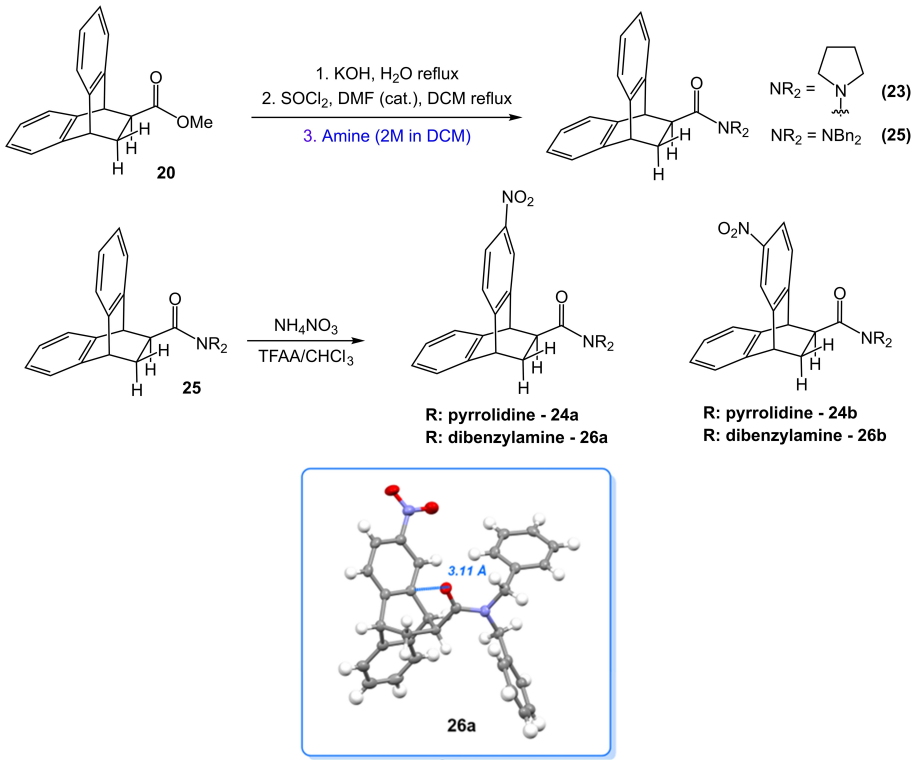

Scheme 13. Synthesis and nitration of compounds **23** and **25** and the X-ray crystal structure of **26a** (50% probability level).

orthogonal to the probe ring. A complex mixture of unreacted, mononitrated and dinitrated products was observed when **27** was treated with 1 equiv. of nitrating agent (Scheme 14).

Precomplexation and transition state calculations

We initially assumed that in most, if not all, cases the directing group stabilizes the forming arenium ion as the electrophile approaches from the opposite face of the aromatic ring (Scheme 3, Type I). However, prior calculational (Figure 3) and an experimental observation (the nitration of the OH group, Scheme 4) prompted us to think something else may be going on. Combining these reasons with the failure of σ-complex analysis, a more rigorous approach to modeling was mandated. To start, we calculated the free energy profiles up to the formation of the putative σ-complexes to understand the roles of various through-space interactions in promoting selectivity. As mentioned above, Singleton has pointed out that the regioselectivity of the aqueous nitration of toluene can be complicated to rationalize and predict, requiring elaborate molecular dynamics simulations (at least for classical nitrations). In our case, we were initially interested in the tractable problem of selectivity between different aromatic rings, which, we believe, can be controlled by precomplexation and a stabilizing relay between the directing group and the substrate aromatic ring (see below). Comparison of relative energies between Wheland intermediates (WI) were investigated with density functional theory (DFT)[40] using Head-Gordon's range-separated functional, ωB97X–D.[41] All other information, including transition-state theory calculations, were computed using Truhlar's hybrid meta-GGA functional, M06-2X[42] (Gaussian 16).

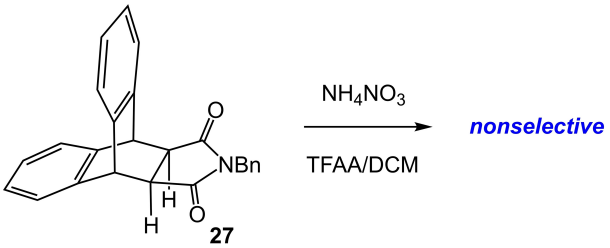

Scheme 14. Nitration of compound **27**.

Halogen and hydroxy directed activation: calculations

We found that the preferred computed pathway for nitration of fluoride **1** involves formation of an exothermic precomplex **1-PC** that lies 1.5 kcal/mol below **1** and free nitronium ($N^+\cdots F$ distance 2.37 Å; Figure 8), followed by transition state **1-TS** through an activation barrier of 3.9 kcal/mol (in free energy) and a $C^+\cdots N$ bond-forming distance of 2.47 Å (NO_2 and F are proximal) to produce the intermediate arenium ion. In contrast, we calculate that nitration of the control ring occurs through endothermic π-complexation (6.2 kcal/mol above **1**), followed by an activation barrier of 4.2 kcal/mol and a $C^+\cdots N$ bond

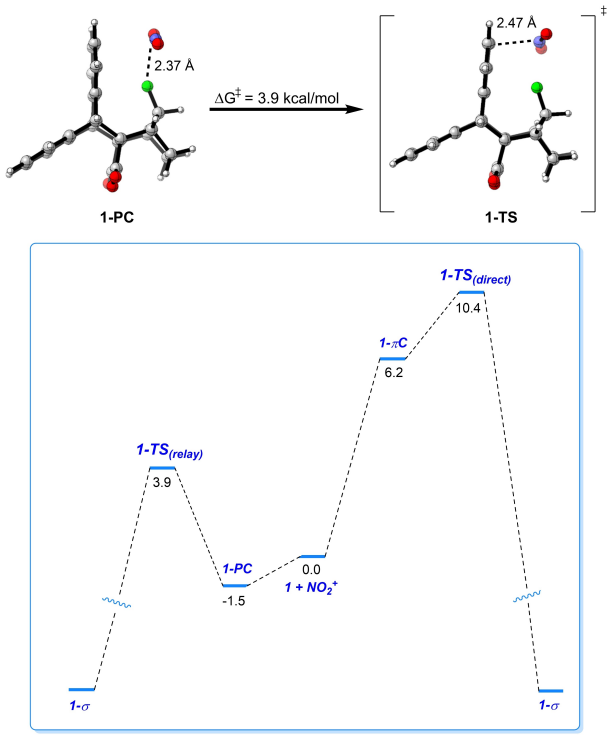

Figure 8. Top: DFT optimized structures of 1-PC (left) and 1-TS (right) computed at (SMD, solvent = DCM) M06-2X/6-311G(d). Bottom: Energy diagram for relay versus direct nitration of 1.

forming distance of 2.72 Å in the transition state. Thus, the experimentally observed selective probe ring nitration can be attributed to a lower activation barrier resulting from the formation of a precomplex in proximity to the aromatic ring, with attendant, *continuous participation* of the directing group through the transition state trajectory. Functionalization is favored on the β-positions of aromatic rings, a fact which is replicated in our calculations for this system and several others.

In further probing the degree of $N^+\cdots F$ interactions, NCI plot analysis[43] of **1-PC** and **1-TS** was performed, which revealed favorable interactions between the nitronium ion and the proximal fluorine as well as the probe ring (Figure 9). QTAIM analysis[44] with a focus upon the computed (3, −1) bond critical point (BCP) highlights fluorine participation in **1-PC** with an aromatic C···F interaction (ρ_{bcp} and $\nabla^2\varrho_{bcp}$ of 0.0172 au and +0.0713 au) and an $N^+\cdots F$ interaction (ρ_{bcp} and $\nabla^2\varrho_{bcp}$ of 0.0214 au and +0.1139 au). A large positive Laplacian value for $N^+\cdots F$ is indicative of an ionic interaction. In the transition state **1-TS**, the $N^+\cdots F$ interaction is weakened, presumably due to an increased bond distance associated with a ρ_{bcp} of 0.0184 au and $\nabla^2\varrho_{bcp}$ of +0.0971 au, while the $N^+\cdots C$ ρ_{bcp} increased to define a new bond path.

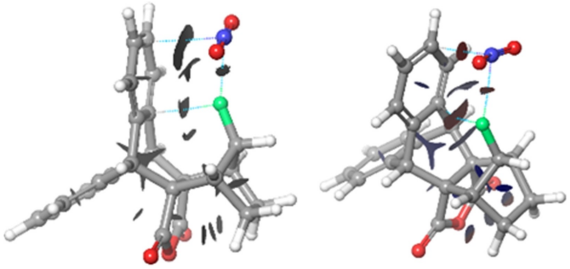

Figure 9. NCI plots of 1-PC (left) and 1-TS (right) computed at (SMD, solvent = DCM) M06-2X/6-311G(d).

In the case of nitrate ester **3**, nitronium is predicted to form the precomplex **3-PC** with an oxygen atom of the nitrate ester ($N^+\cdots O$ distance 2.42 Å) that lies 0.03 kcal/mol below **3**. Therefrom it is directed to react with the *syn* face of the aromatic ring, forming the corresponding arenium ion. This process occurs through **3-TS**, with an activation barrier of 1.7 kcal/mol and an $N^+\cdots C$ bond-forming distance of 2.46 Å. Despite the electron withdrawing nature of the nitrate group, a relay pathway is still favored over direct nitration of the control ring. In fact, the activation barrier for nitration of the control ring is found to be 6.7 kcal/mol ($\Delta G^{\ddagger}$ = 3.9 kcal/mol) above starting material. Note that in the case of bromination, the hydroxy group remains unfunctionalized, and is thus a better activator for sequential probe ring brominations.[3a]

For scaffold II, the situation is more ambiguous. Consider the nitration of fluoride **10**. The position of the fluorine atom with respect to the probe aromatic ring (slid down to align with its bottom edge, Figure 10) makes it an unlikely anchor to relay nitronium to the two reactive positions on the top. Calculations confirm the absence of a significant interaction between fluorine and nitronium in **10-TS**. Stabilization is instead coming from a direct *syn* interaction of the aromatic ring with the fluorine atom. On the other hand, the control ring is nonideal. Aromatic substitution is destabilized by virtue of a prominent π→σ*(C–F) interaction (Figure 10). The same analysis applies for chloride **12**. In bromide **15**, the deactivating presence of the

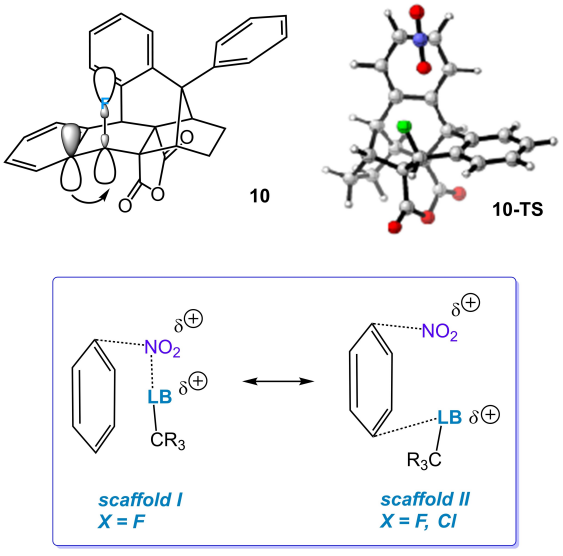

Figure 10. Top left: Deactivating interaction between π→σ*(C–F) in 10. Top right. Transition state 10-TS revealing lack of a strong relay effect. Bottom: Switch in mode of activation from scaffold I to II.

preinstalled bromine atom on the probe ring forces nitration to the third aromatic ring.

Tetrazoles: calculations

The situation is different and more interesting in the nitration of tetrazole **18**. We anticipated a rotationally mobile tetrazole unit may direct nitration to all four available positions of the probe ring by "sweeping" over the surface of the aromatic system as seen from Figure 11(a). In our initial computational investigation, subjected the two most stable rotational isomers of **18** to nitration of the arene ring. A very strong relay effect from the tetrazole moiety to the probe aromatic ring was displayed (Figure 11b) with **18-pc** lying 10 kcal/mol below the starting material and a tetrazole-nitronium $N^3\cdots N^+$ distance of 2.29 Å. From **18-pc**, nitration of the arene ring proceeds through **18-ts** ($\Delta G^{\ddagger} = 6.4$ kcal/mol) along the reaction coordinate with noticeable elongation of the $N^3\cdots N^+$ distance to 2.58 Å and a $C\cdots N^+$ bond forming distance of 2.37 Å. In contrast, nitration of the control ring is a slightly endergonic process with the transition state leading to nitration of the π-system lying 2.1 kcal/mol above the starting materials and ~6 kcal/mol relative to **18-ts**. Thus, a strong electrostatic interaction displayed in **18-pc** between the nitronium cation and electron-rich tetrazole group is indicative of a clear relay effect through the mechanism. Finally, although the calculational model favors β-substitution, α-substitution (seen to a very small extent) is also energetically accessible, thus favoring the relay mechanism.

Carbonyl directed activation: calculations

In contrast to the carbonyl group in **8**, those in diester **21** align well for precomplexation. When a 1:1 mixture of **21** and **28** (the epimer of **21** with *trans* ester groups) is treated with 1 equiv. of nitrating agent, integration of relevant peaks in the

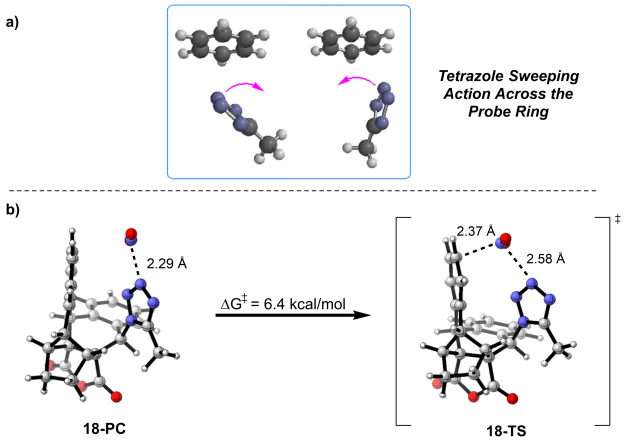

Figure 11. a) Sweeping action of the tetrazole moiety across the probe aromatic ring; b) precomplex and transition state revealing a strong relay effect.

^{1}H NMR of the reaction mixture showed four times more nitrated products of the *cis*-diester **21** than the *trans*-diester **28**, pointing to a role for neighboring group assistance. These factors led us to examine reaction pathways for **21** and **28** in detail.

Nitronium ion can form two different types of π-complexes with compound **21** (Figure 12, right). A typical π-complex[45–47] involving the unperturbed ring (**22b-PC** wherein the nitronium ion is perpendicular to the ring) is located 10.9 kcal/mol higher in free energy than **21**. From this precomplex, **22b** undergoes NO_2^+ coordination with the π-system on the unperturbed ring through **22b-TS**, which lies 0.1 kcal/mol above **22b-PC** and 11.0 kcal/mol above **21** on the reaction coordinate. In contrast, the electron-rich ester carbonyl groups can interact with the nitronium ion to form precomplex **22a-PC**, containing a $O\cdots N^+$ distance of 2.37 Å that is predicted to be 9.3 kcal/mol lower in energy than **21**. From this precomplex, **22a-PC** surmounts transition state **22a-TS** with a $C\cdots N^+$ bond forming distance of 2.44 Å that lies 7.5 kcal/mol above **22a-PC** and 1.8 kcal/mol below **21** on the reaction coordinate. *Notably, these computed trends for nitration are consistent with the selectivity observed experimentally.*

Although the trans-diester **28** is 2.1 kcal/mol more stable than the cis-diester **21**, the cis precomplex **22a-PC** is much lower in energy than the trans precomplex **28a-PC**, which lies 4.9 kcal/mol below **28**. This precomplex proceeds to form the σ-complex **28a** through **28a-TS** that lies 2.1 kcal/mol above **28** ($\Delta G^{\ddagger} = 7.0$ kcal/mol, Figure 12, left). The binding energy ΔG is 4.4 kcal/mol lower for the formation of **22a-PC** implying that in solution, concentration of the cis π-complex is higher than the trans π-complex, and leads to higher amounts of cis-nitrated products.

NCI analysis on both the precomplex **22a-PC** and the transition state **22a-TS** revealed arene stabilization by the ester carbonyl group, along with a strong cation-π interaction between the aromatic ring and nitronium. The presence of an additional ester moiety aids in stabilizing the aromatic cation, at the cost of repulsive interactions with the adjacent ester group. QTAIM analysis of **22a-PC** reveals the presence of a BCP with a $\boldsymbol{\rho}_{\mathbf{bcp}}$ and $\nabla^2\rho_{bcp}$ values of 0.0244 au and +0.1264, identifying an ionic interaction between the ester carbonyl and nitronium. The arene ring is seen to have a weak electrostatic interaction with both the nitronium ion and the carbonyl that strengthens in the TS.

Turning to amide activation, the optimal pathway for the formation of **24b** was found to proceed *through* precomplex **24b-PC** lying 12 kcal/mol below starting materials ($N^+\cdots O$ distance of 2.26 Å), followed by transition state **24b-TS**, with an activation barrier of 6.7 kcal/mol ($C^+\cdots N$ bond-forming distance of 2.42 Å). In contrast, nitration of the control ring proceeds through π-complexation of the nitronium ion with the aromatic system associated with an activation barrier of 7.3 kcal/mol and $C^+\cdots N$ bond-forming distance of 2.76 Å. Once again, nitration by a relay process with an amide directing group is favored over π-complexation with the aromatic system.

Directly visible from the NCI plots was the presence of weak interactions between the carbonyl oxygen and the nitronium

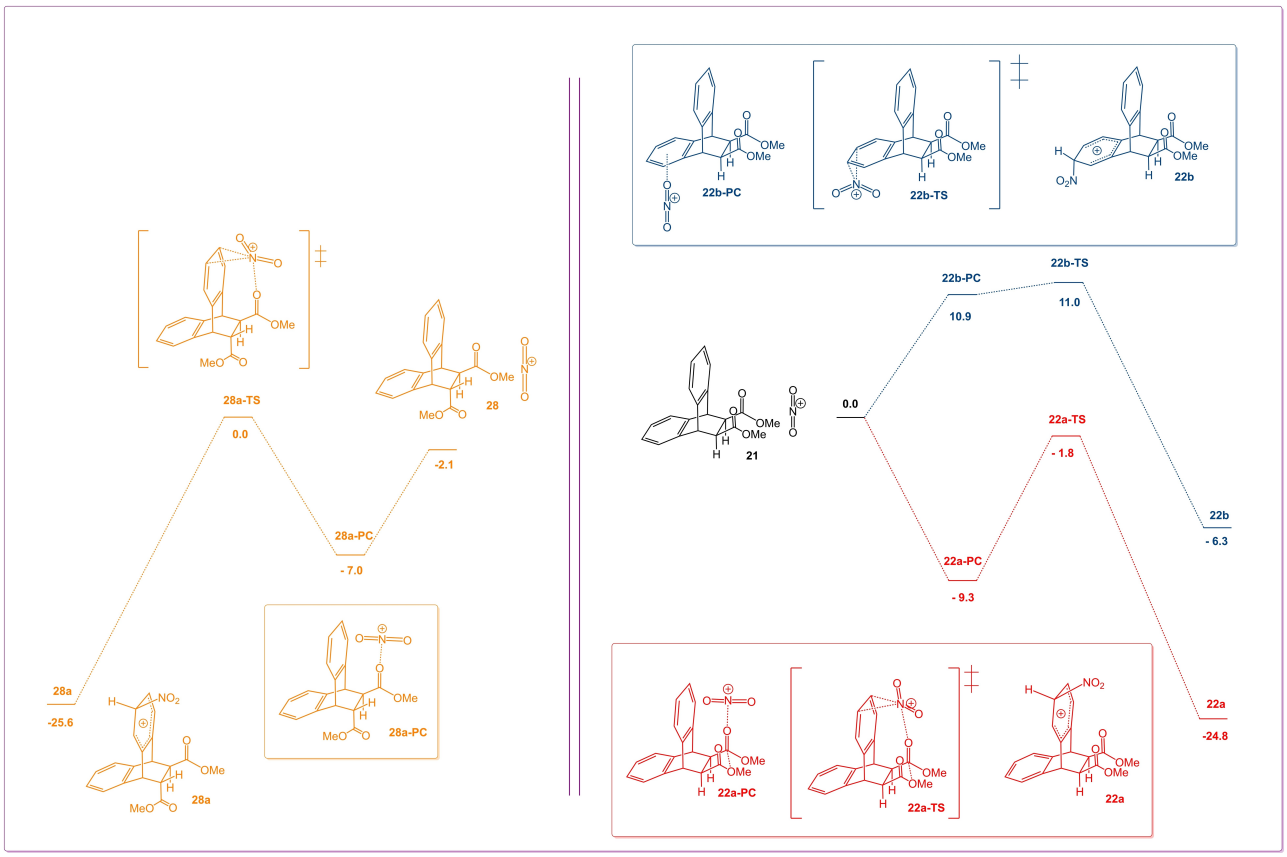

Figure 12. Free energy profile (M06-2X/6-311G(d) SMD [CH_2Cl_2]) up to the formation of σ complexes in cis- and trans-diesters **21** and **28** involving precomplexes and transition states. Nitration of the trans-diester **28** has previously been reported (Supporting Information of Ref. [9]).

ion as well as cation-π interactions between the probe arene ring and nitronium. Similarly, QTAIM analysis also depicts strong $N^+\cdots O$ interactions in **24b-PC** that decrease in **24b-TS**, whereas $C_\pi\cdots N^+$ interactions increase from **24b-PC** to **24b-TS**.

This system presents an interesting case of positional selectivity. DFT predicts two nitrated regioisomers from σ-complexes on the probe ring, **24a** and **24b**. Initial examination of the two σ-complexes revealed a significant energy difference, **24b** being ~15 kcal/mol more stable than **24a**. Interestingly, the activation energy for **24b-TS** was found to be slightly *higher* ($\Delta G^{\ddagger} = 6.7$ kcal/mol) compared to **24a-TS** ($\Delta G^{\ddagger} = 5.3$ kcal/mol). This negligible difference in activation energies corroborates the experimental ratio of ~1:1 observed for regioisomers **24a** and **24b**. As mentioned above, Singleton has pointed out that the regioselectivity of nitration can be complicated to rationalize and predict, requiring elaborate molecular dynamics simulations. In our case, subtle energy differences between precomplexes and activation energies of the corresponding transition states can provide a rationale for the observed regioselectivity to an extent.

Conclusions

We have established that halogens, tetrazoles, esters and amides can direct electrophilic substitutions to nearby aromatic rings through stabilized "relay" tranisition states. Rigidity, propinquity, and Lewis basicity are commanding factors in determining the relay effect. However, when the through-space directing group is less than optimally positioned with respect to the probe aromatic rings, the relay effect may be absent or altered. This new model helps rationalize these transformations and could be of predictive value. In effect, these heretofore unexplored interactions provide an alternative platform to design aromatic systems, including drug candidates, materials, etc. that are otherwise difficult to synthesize with traditional aromatic substitution reactions.

Supporting Information

Synthetic procedures, X-ray crystallographic analysis data, NMR spectra, and computational information are included in the Supporting Information.

Deposit Numbers 2209570 (for **10**), 2209571 (for **11a**), 2209569 (for **11b**), 2209573 (for **12**), 2209572 (for **13**), 2209590 (for **15**), 2209589 (for **16**), 2209591 (for **18**), 2209592 (for **19a**),

2209593 (for **19b**), 2209579 (for **26a**), and 2209580 (for **26b**) contain the supplementary crystallographic data for this paper. These data are provided free of charge by the joint Cambridge Crystallographic Data Centre and Fachinformationszentrum Karlsruhe Access Structure service.

Additional references cited within supporting information.[48–59]

Acknowledgements

T.L. thanks the National Science Foundation (Grant CHE 2102116) for financial support. Z.F. and D.J.T. thank the National Science Foundation (Grant CHE-1856416) for financial support and XSEDE for computational support. Mass spectral data were obtained at the University of Delaware's center. T.D. thanks the Natural Sciences and Engineering Research Council of Canada for Discovery Grants (RGPIN-2019-04205). Computations were carried out using facilities at Digital Research Alliance of Canada; this research was enabled in part by support provided by SHARCNET (Shared Hierarchical Academic Research Computing Network) and Compute/Calcul Canada and the Digital Research Alliance of Canada. S.V. acknowledges QEII-GSST.

Conflict of Interests

The authors declare no conflict of interest.

Data Availability Statement

The data that support the findings of this study are available in the supplementary material of this article.

Keywords: density functional theory · electrophilic substitution · fluorine · noncovalent interactions · pre-complexation

[1] L. N. Ferguson, *Chem. Rev.* **1952**, *50*, 47–67.
[2] B. Galabov, D. Nalbantova, P. V. Schleyer, H. F. Schaefer, *Acc. Chem. Res.* **2016**, *49*, 1191–1199.
[3] a) L. Guan, M. G. Holl, C. R. Pitts, M. D. Struble, M. A. Siegler, T. Lectka, *J. Am. Chem. Soc.* **2017**, *139*, 14913–14916; b) M. Kazim, L. Guan, A. Chopra, R. Sun, M. A. Siegler, T. Lectka, *J. Org. Chem.* **2020**, *85*, 9801–9807.
[4] a) M. G. Holl, M. D. Struble, P. Singal, M. A. Siegler, T. Lectka, *Angew. Chem. Int. Ed.* **2016**, *55*, 8266–8269; b) For a study of lone-pair–π interactions, see; J. Novotny, S. Bazzi, R. Marek, J. Kozelka, *Phys. Chem. Chem. Phys.* **2016**, *18*, 19472–19481.
[5] G. W. Wheland, *J. Am. Chem. Soc.* **1942**, *64*, 900–908.
[6] J. Y. Wang, K. Choi, S. J. Zuend, K. Borate, H. Shinde, R. Goetz, J. F. Hartwig, *Angew. Chem. Int. Ed.* **2021**, *60*, 399–408.
[7] A. C. Knipe, J. Loundkeast, N. Sridhar, *J. Chem. Soc. Chem. Commun.* **1976**, 765–766.
[8] N. Stamenkovic, N. P. Ulrih, J. Cerkovnik, *Phys. Chem. Chem. Phys.* **2021**, *23*, 5051–5068.
[9] K. E. Murphy, J. L. Bocanegra, X. X. Liu, H. Y. K. Chau, P. C. Lee, J. N. Li, S. T. Schneebeli, *Nat. Commun.* **2017**, *8*, 14840.
[10] J. P. Campbell, S. C. Rajappan, T. J. Jaynes, M. Sharafi, Y. T. Ma, J. Li, S. T. Schneebeli, *Angew. Chem. Int. Ed.* **2019**, *58*, 1035–1040.
[11] J. P. Campbell, M. Sharafi, K. E. Murphy, J. L. Bocanegra, S. T. Schneebeli, *Supramol. Chem.* **2019**, *31*, 565–574.
[12] M. Sharafi, J. P. Campbell, K. E. Murphy, R. O. Brown, S. T. Schneebeli, *Synlett* **2021**, *32*, 229–234.
[13] Y. N. Quinones, D. A. Singleton, *J. Am. Chem. Soc.* **2016**, *138*, 15167–15176.
[14] M. Kazim, M. A. Siegler, T. Lectka, *T. Org. Lett.* **2019**, *21*, 2326–2329.
[15] R. Bhatia, K. Kadyan, M. Duhan, M. Devi, R. Singh, R. C. Kamboj, P. Kumar, *ChemistrySelect* **2019**, *4*, 10417–10424.
[16] S. Z. Zard, *Chem. Commun.* **2002**, 1555–1563.
[17] R. N. Grimes, *J. Organomet. Chem.* **2013**, *747*, 4–15.
[18] H. E. Ho, A. Pagano, J. R. Ashton, J. R. Donald, R. G. Epton, J. C. Churchill, M. J. James, P. O'Brien, R. J. K. Taylor, W. P. Unsworth, *Chem. Sci.* **2020**, *11*, 1353–1360.
[19] M. Kazim, M. A. Siegler, T. Lectka, *J. Org. Chem.* **2019**, *84*, 15765–15765.
[20] J. V. Crivello, *J. Org. Chem.* **1981**, *46*, 3056–3060.
[21] A. S. Mahadevi, G. N. Sastry, *Chem. Rev.* **2013**, *113*, 2100–2138.
[22] J. A. Faraldos, A. K. Antonczak, V. Gonzalez, R. Fullerton, E. M. Tippmann, R. K. Allemann, *J. Am. Chem. Soc.* **2011**, *133*, 13906–13909.
[23] D. A. Dougherty, *Acc. Chem. Res.* **2012**, *46*, 885–893.
[24] H. Reed, T. R. Paul, W. J. Chain, *J. Org. Chem.* **2018**, *83*, 11359–11368.
[25] R. J. Herr, *Bioorg. Med. Chem.* **2002**, *10*, 3379–3393.
[26] P. Kushwaha, S. Fatima, A. Upadhyay, S. Gupta, S. Bhagwati, T. Baghel, M. I. Siddiqi, A. Nazir, K. V. Sashidhara, *Bioorg. Med. Chem. Lett.* **2019**, *29*, 66–72.
[27] Y. J. Li, K. K. Pasunooti, R. J. Li, W. K. Liu, S. A. Head, W. Q. Shi, J. O. Liu, *J. Med. Chem.* **2018**, *61*, 11158–11168.
[28] J. Y. Zhang, S. Wang, Y. Y. Ba, Z. Xu, *Eur. J. Med. Chem.* **2019**, *178*, 341–351.
[29] F. Gao, J. Q. Xiao, G. Huang, *Eur. J. Med. Chem.* **2019**, *184*, 111744.
[30] S. Q. Wang, Y. F. Wang, Z. Xu, *Eur. J. Med. Chem.* **2019**, *170*, 225–234.
[31] P. Lassalas, G. Gay, C. Lasfargeas, M. J. James, V. Tran, K. G. Vijayendran, K. R. Brunden, M. C. Kozlowski, C. J. Thomas, A. B. Smith, D. M. Huryn, C. Ballatore, *J. Med. Chem.* **2016**, *59*, 3183–3203.
[32] J. Roh, G. Karabanovich, H. Vlckova, A. Carazo, J. Nemecek, P. Sychra, L. Valaskova, O. Pavlis, J. Stolarikova, V. Klimesova, K. Vavrova, P. Pavek, A. Hrabalek, *Bioorg. Med. Chem.* **2017**, *25*, 5468–5476.
[33] A. M. Okljesa, O. R. Klisuric, *J. Mol. Struct.* **2021**, *1226*, 129341.
[34] P. D. Bartlett, F. A. Tate, *J. Am. Chem. Soc.* **1953**, *75*, 91–95.
[35] H. G. Oddy, *J. Am. Chem. Soc.* **1923**, *45*, 2156–2160.
[36] A. Kumar, G. Wagner, R. R. Ernst, K. Wuthrich, *J. Am. Chem. Soc.* **1981**, *103*, 3654–3658.
[37] R. Horst, G. Wider, J. Fiaux, E. B. Bertelsen, A. L. Horwich, K. Wuthrich, *Proc. Natl. Acad. Sci. USA* **2006**, *103*, 15445–15450.
[38] B. J. Marsh, H. Adams, M. D. Barker, I. U. Kutama, S. Jones, *Org. Lett.* **2014**, *16*, 3780–3783.
[39] S. Arya, S. Kumar, R. Rani, N. Kumar, P. Roy, S. M. Sondhi, *Med. Chem. Res.* **2013**, *22*, 4278–4285.
[40] a) P. Hohenberg, W. Kohn, *Phys. Rev.* **1964**. *136* B864-B71; b) W. Kohn, L. J. Sham, *Phys. Rev.* **1965** *140* A1133-A38; c) R. G. Parr, W. Yang, *Oxford Univ. Press*, Oxford, **1989**.
[41] Y. Zhao, D. G. Truhlar, *Theor. Chem. Acc.* **2008**, *120*, 215–241.
[42] J. D. Chai, M. Head-Gordon, *Phys. Chem. Chem. Phys.* **2008**, *10*, 6615–6620.
[43] J. C. Garcia, E. R. Johnson, S. Keinan, R. Chaudret, J. P. Piquemal, D. N. Beratan, W. Yang, *J. Chem. Theory Comput.* **2011**, *7*, 625–632.
[44] R. F. W. Bader, *Acc. Chem. Res.* **1985**, *18*, 9–15.
[45] G. A. Olah, *Acc. Chem. Res.* **1971**, *4*, 240–248.
[46] G. A. Olah, N. A. Overchuk, *Can. J. Chem.* **1965**, *43*, 3279–3293.
[47] G. A. Olah, S. J. Kuhn, S. H. Flood, *J. Am. Chem. Soc.* **1961**, *83*, 4571–4580.
[48] Gaussian 16, Revision C.01, M. J. Frisch, G. W. Trucks, H. B. Schlegel, G. E. Scuseria, M. A. Robb, J. R. Cheeseman, G. Scalmani, V. Barone, G. A. Petersson, H. Nakatsuji, X. Li, M. Caricato, A. V. Marenich, J. Bloino, B. G. Janesko, R. Gomperts, B. Mennucci, H. P. Hratchian, J. V. Ortiz, A. F. Izmaylov, J. L. Sonnenberg, D. Williams-Young, F. Ding, F. Lipparini, F. Egidi, J. Goings, B. Peng, A. Petrone, T. Henderson, D. Ranasinghe, V. G. Zakrzewski, J. Gao, N. Rega, G. Zheng, W. Liang, M. Hada, M. Ehara, K. Toyota, R. Fukuda, J. Hasegawa, M. Ishida, T. Nakajima, Y. Honda, O. Kitao, H. Nakai, T. Vreven, K. Throssell, J. A. Jr. Montgomery, J. E. Peralta, F. Ogliaro, M. J. Bearpark, J. J. Heyd, E. N. Brothers, K. N. Kudin, V. N. Staroverov, T. A. Keith, R. Kobayashi, J. Normand, K. Raghavachari, A. P. Rendell, J. C. Burant, S. S. Iyengar, J. Tomasi, M. Cossi, J. M. Millam, M. Klene, C. Adamo, R. Cammi, J. W. Ochterski, R. L. Martin, K. Morokuma, O. Farkas, J. B. Foresman, D. J. Fox, Gaussian, Inc., Wallingford CT, **2016**.

[49] Schrödinger Release 2019 – 2: Jaguar; Schrödinger, LLC: New York, **2019**.
[50] Y. Zhao, D. G. Truhlar, *Theor. Chem. Acc.* **2008**, *120*, 215–241.
[51] A. V. Marenich, C. J. Cramer, D. G. Truhlar, *J. Phys. Chem. B.* **2009**, *113*, 6378–6396.
[52] J. D. Chai, M. Head-Gordon, *Phys. Chem. Chem. Phys.* **2008**, *10*, 6615–6620.
[53] C. Gonzalez, H. B. Schlegel, *J. Phys. Chem.* **1990**, *94*, 5523–5527.
[54] K. Ukui, *Acc. Chem. Res.* **1981**, *14*, 363–368.
[55] C. Y. Legault, CYLview, version 1.0b; Universite de Sherbrooke: Quebec, Canada, 2009, http://www.cylview.org.
[56] R. Dennington, T. A. Keith, J. M. Millam, GaussView, Version 6.1; Semichem Inc., Shawnee Mission, KS, 2016.
[57] Schrödinger Release 2018–4: Jaguar, Schrödinger, LLC, New York, NY, 2018.
[58] T. A. Keith, AIMAll (Version 17.11.14), TK Gristmill Software, Overland Park, KS 2017. http://aim.tkgristmill.com.
[59] a) N. Suma, D. Aruldhas, I. H. Joe, A. R. Anuf, B. A. Sasi, *J. Mol. Struct.* **2020**, *1206*, 127677; b) R. Hossain, M. Hasan, M. Nishat, F. Ahmed, T. Ferdous, M. A. Hossain, *J. Mol. Liq.* **2021**, 114627.

Manuscript received: May 17, 2023
Accepted manuscript online: May 23, 2023
Version of record online: ■■, ■■

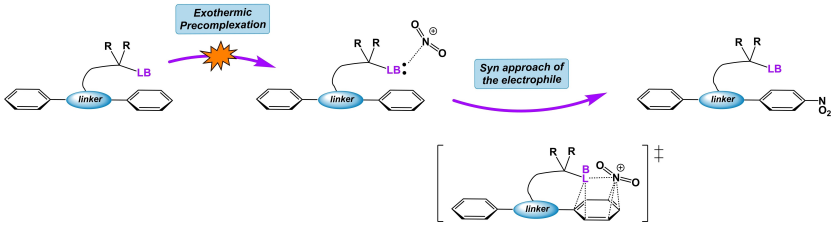

Dr. M. Kazim, Z. Feng, S. Vemulapalli, Dr. M. A. Siegler, A. Chopra, P. Minh Nguyen, Dr. M. Gargiulo Holl, Dr. L. Guan, Prof. T. Dudding, Prof. D. J. Tantillo*, Prof. T. Lectka**

1 – 13

Through-Space, Lone-Pair Promoted Aromatic Substitution: A Relay Mechanism Can Beat Out Direct Activation

Through stabilized "relay" tranisition states: Various Lewis basic functional groups can spatially activate aromatic substitutions. Mechanistically, these reactions proceed through an exothermic relay pathway, as opposed to the previously assumed endothermic direct activation. In this article, both experimental and theoretical models are employed to investigate this newly discovered mode of arene activation in detail.